

# Study of Dynamic Range Limits of SKA Images

Maxim Voronkov, Mark Wieringa

CSIRO ATNF

## Abstract

We present a study of the dynamic range which can be reached for images produced with the SKA. Results of simulations carried out for one spiral layout (SKA concept description, June 2002) has shown that AIPS++ Clark CLEAN provides a dynamic range decreasing rapidly with the distance from the phase-tracking centre. Presumably, the most severe effect on the dynamic range is due to gridding and aliasing at the imaging stage. The Cotton-Schwab CLEAN where the model subtraction is performed in the visibility domain gives a constant dynamic range of about  $10^8$  or higher if one takes into consideration  $w$ -term in the relation between the sky brightness and visibilities while forming the model.

## 1 Introduction

Dynamic range is one of the most important characteristics of the future generation radio telescope like the SKA. There will be a huge number of bright sources in the large field of view of such an instrument and high dynamic range is necessary if one wants to study weak sources. Unfortunately, simulations are almost the only method to estimate this characteristic because it depends not only on the layout of antennas but also on the method of data processing, most of which are difficult to study analytically. To be an efficient instrument the SKA should have a dynamic range of the order of  $10^6 - 10^7$ . The goal of this work is to study what dynamic range could be reached for the simplest case of a single point source without any noise.

## 2 Simulations

Simulations were carried out in the AIPS++ environment. An approximated flow-chart is shown in Fig.1. First, visibilities for the model of a single point source without any noise were created using the AIPS++ simulator tool. All simulations were done for

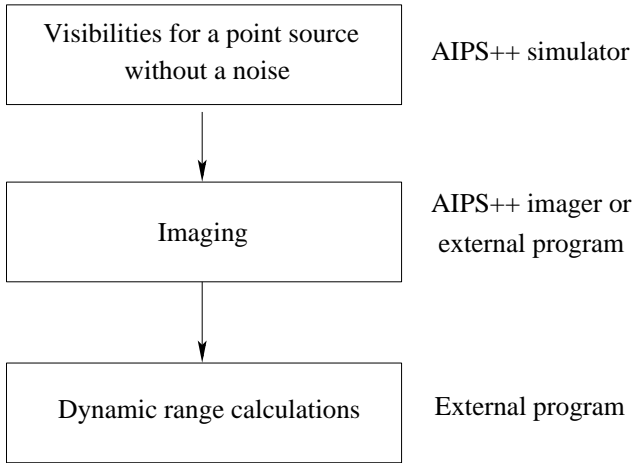


Figure 1: Simulations Flow-chart

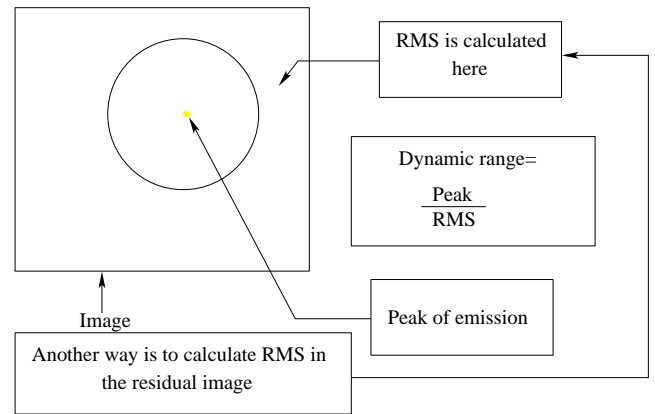


Figure 2: Dynamic range calculations

the same spiral layout (SKA concept description, June 2002), for an equatorial source at 8 GHz. A simulated dataset was a snap-shot containing one visibility sample per baseline and one frequency channel only. At the second stage the imaging of the dataset was performed using either standard AIPS++ algorithms or an external program. A result of the imaging stage was analyzed by the external program to assess the image fidelity. It is possible to characterize a fidelity of the image in two ways. First, we may take a restored image which is a result of CLEAN algorithm, find a pixel with a maximum brightness, circumscribe a circle of some radius centered at this pixel and calculate a dynamic range as a ratio of the maximum brightness found in the image to the rms brightness calculated using all pixels outside the circle (see Fig.2). Another possibility is to calculate rms brightness using all pixels in residual image and use the peak brightness known a-priori. For the standard AIPS++ Clark CLEAN both methods give the dynamic range of the same order. An advantage of the first approach is in its possibility to assess the image fidelity at different distances from the peak source. If a deconvolution algorithm experienced some problems (e.g. ordinary CLEAN works badly when a point spread function has extended wings) the noise level in the resulting image may be different in the regions near the simulated source and far away from it. As a drawback, this method is useless in the case of more complicated model of the sky brightness like a set of point sources, requires more computational resources, and requires a guess about the circle radius if we would like to have one number only. If we are confident that a deconvolution algorithm works pretty well it is safe to use the second approach. In addition, it allows us to avoid additional errors introduced by the image restoration, e.g. gridding errors originating from the FFT-convolution with a restoring beam. Everywhere in this work, except the study of the weighting effects,

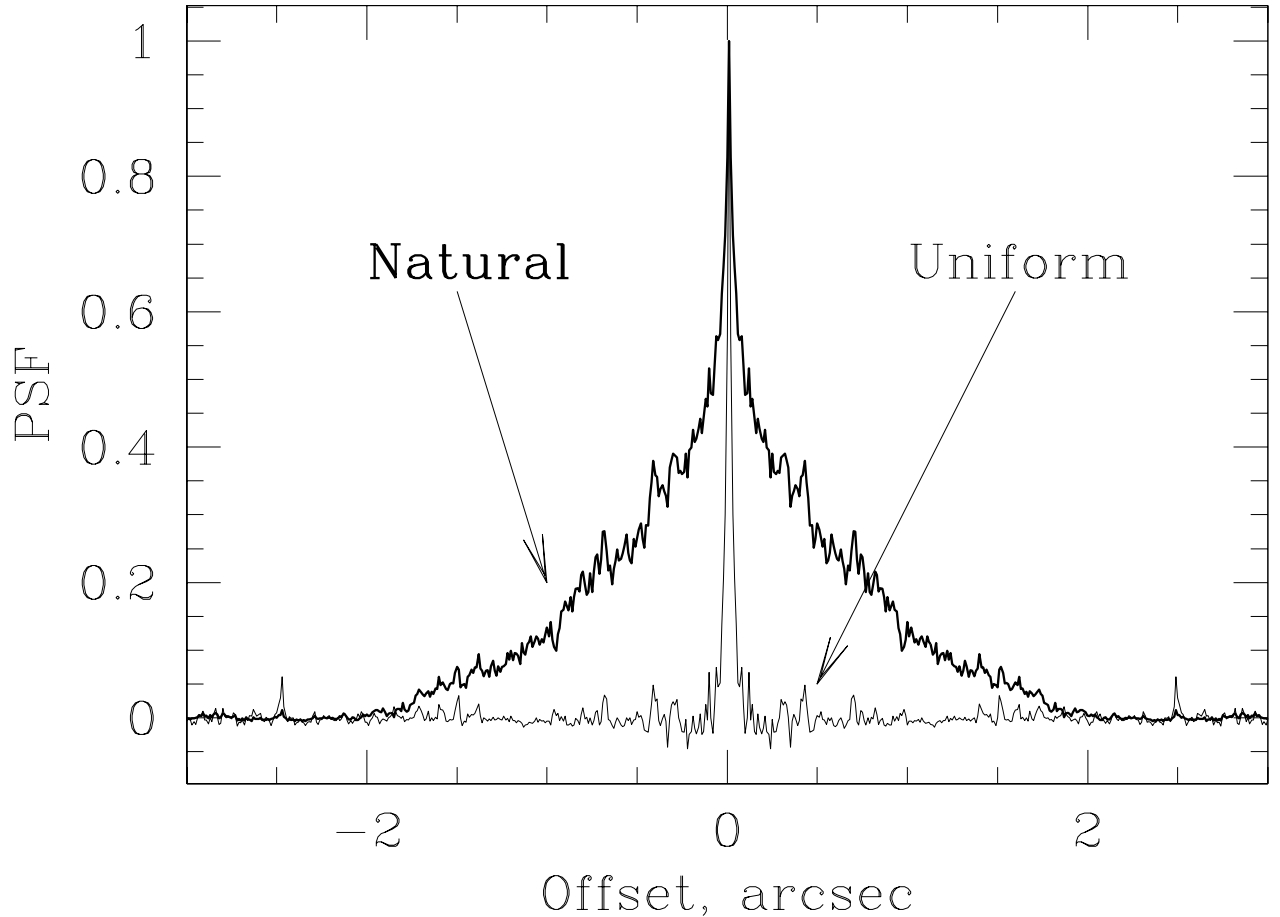


Figure 3: Slices of the Point Spread Function for the case of the uniform and natural weighting schemes.

we calculated the dynamic range as a ratio of the peak brightness which was known a-priori to the rms noise in the residual image.

## 3 Results

### 3.1 Weighting schemes

Due to a limited  $uv$ -coverage in the case of short observations and a single frequency channel some regions on the  $uv$ -plane will be unsampled producing sidelobes in the Point Spread Function. The magnitude of these sidelobes will determine the dynamic range of the dirty image. Deconvolution stage is necessary to clean up such sidelobes and hence to increase the dynamic range. In this case the dynamic range depends on

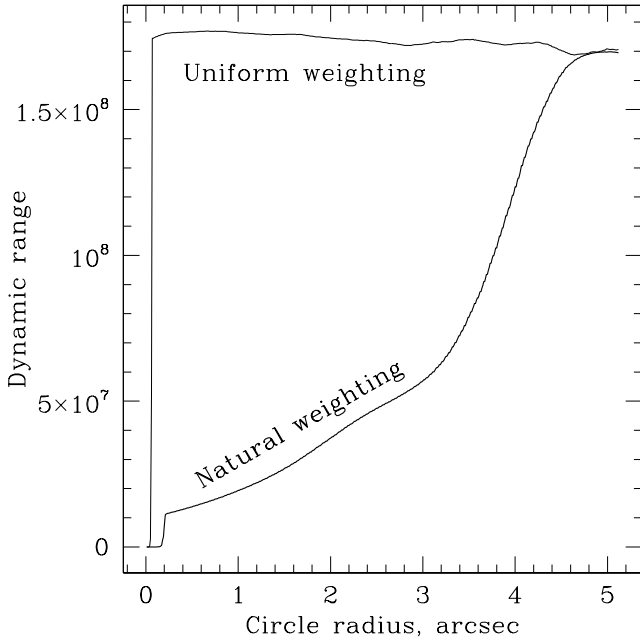


Figure 4: Dynamic range versus the circle radius (Fig.2) after standard AIPS++ Clark Clean.

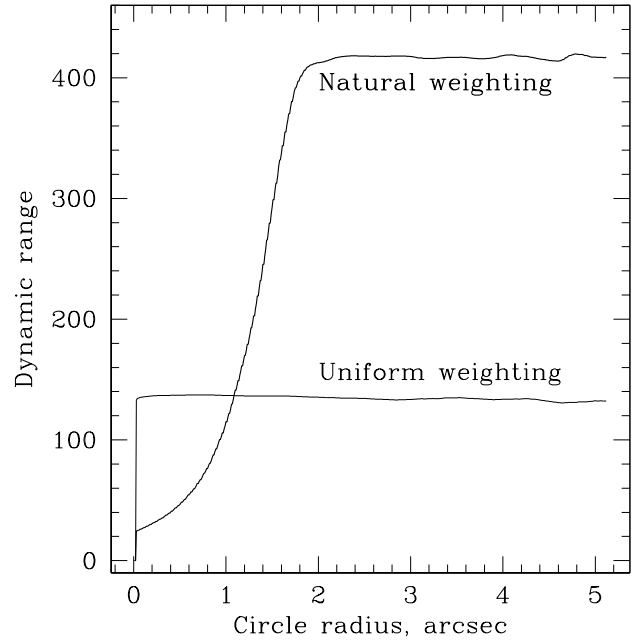


Figure 5: The same as in Fig.4 but for dirty image.

the efficiency of the deconvolution algorithm. Simulations are almost the only way to analyze how well the deconvolution works for different shapes of the dirty beam. It is known that the CLEAN algorithm usually experiences difficulties deconvolving the image when the point spread function has extended wings. Such a beam shape is typical when the number of short baselines is large compared to the number of long baselines. This is the situation we have for the spiral SKA layout (SKA concept description, June 2002). The beam shape can be controlled by applying different weighting schemes. For example, in the case of natural weighting each visibility sample is assigned a weight corresponding to the error of the respective measurement. In this simulation it means that all weights are equal to unity because no noise has been added. Natural weighting maximizes the image sensitivity but the point spread function has extended wings decreasing the resolution (see Fig.3). Uniform weighting equalizes the density of measurements in  $uv$ -plane alleviating the influence of the short baselines. It corresponds to the case of larger resolution but the sensitivity becomes worse because it redistributes the power from the extended wings of the natural weighted point spread function into random noise of the uniform weighted synthesized beam (see Fig.3). For more information regarding weighting schemes see Briggs' thesis (1995).

Results of simulations presented in Fig.4 and 5. An extended halo around the simulated point source exists in the cleaned image for the case of the natural weighting

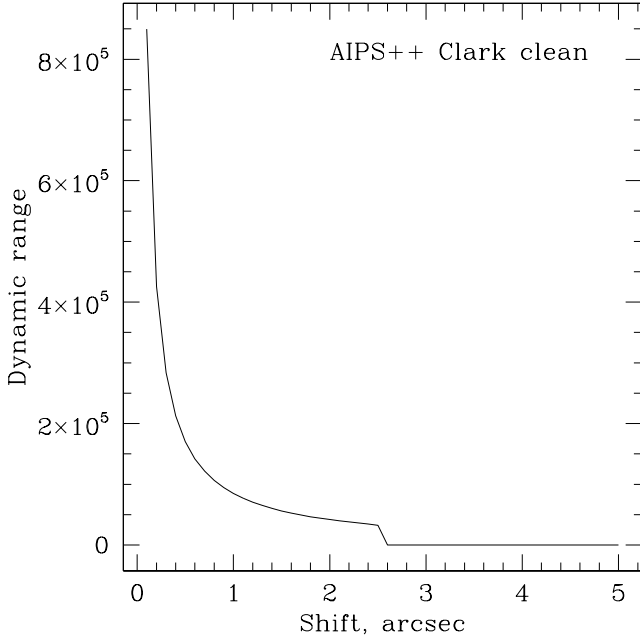


Figure 6: Dynamic range versus the offset from the phase centre. Standard AIPS++ Clark CLEAN. The step in the curve near the center of the plot corresponds to the inner quarter of the image where algorithm actually works.

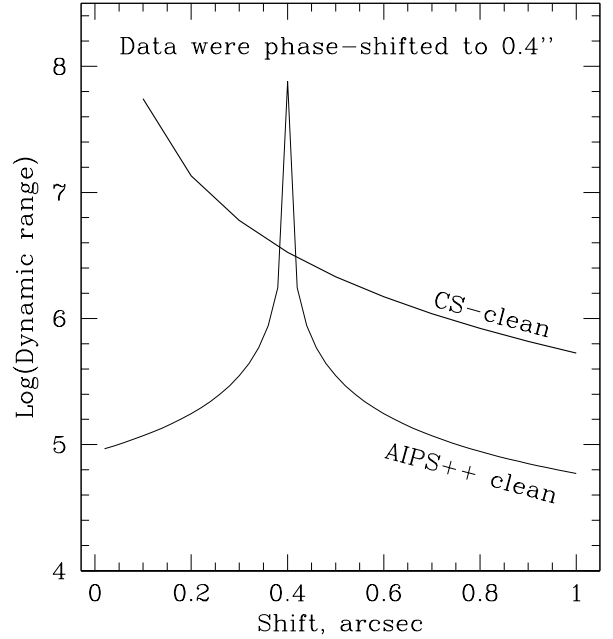


Figure 7: The same as in Fig.6 but visibility dataset was phase-shifted to 0.4 arcsec. Two curves represent the behavior of the AIPS++ Clark CLEAN and Cotton-Schwab CLEAN. Scale is logarithmic.

decreasing a dynamic range. At a large distance from the peak of the emission the two weighting schemes give similar dynamic ranges (Fig.4). We would expect uniform weighting to give higher sidelobes and hence lower dynamic range. This reflects the difficulty the standard CLEAN algorithm has with a point spread function with extended wings. For the dirty images, i.e. without deconvolution, natural weighting gives about 3 times greater dynamic range far away from the point source (Fig.5).

### 3.2 Off-axis dynamic range

Previous experiments were devoted to the case where the simulated point source is located at the phase-tracking centre. Results in this section will address the case when the source has an offset from that. It is convenient to analyze the algorithm behavior using the plots of the dynamic range on the offset from the phase-tracking centre. As can be seen in Fig.6, for the standard AIPS++ Clark CLEAN the dynamic range decreases rapidly with a distance from the phase-tracking centre. It is important to understand this effect before modeling of a more complex sky brightness. Even in the case of two point

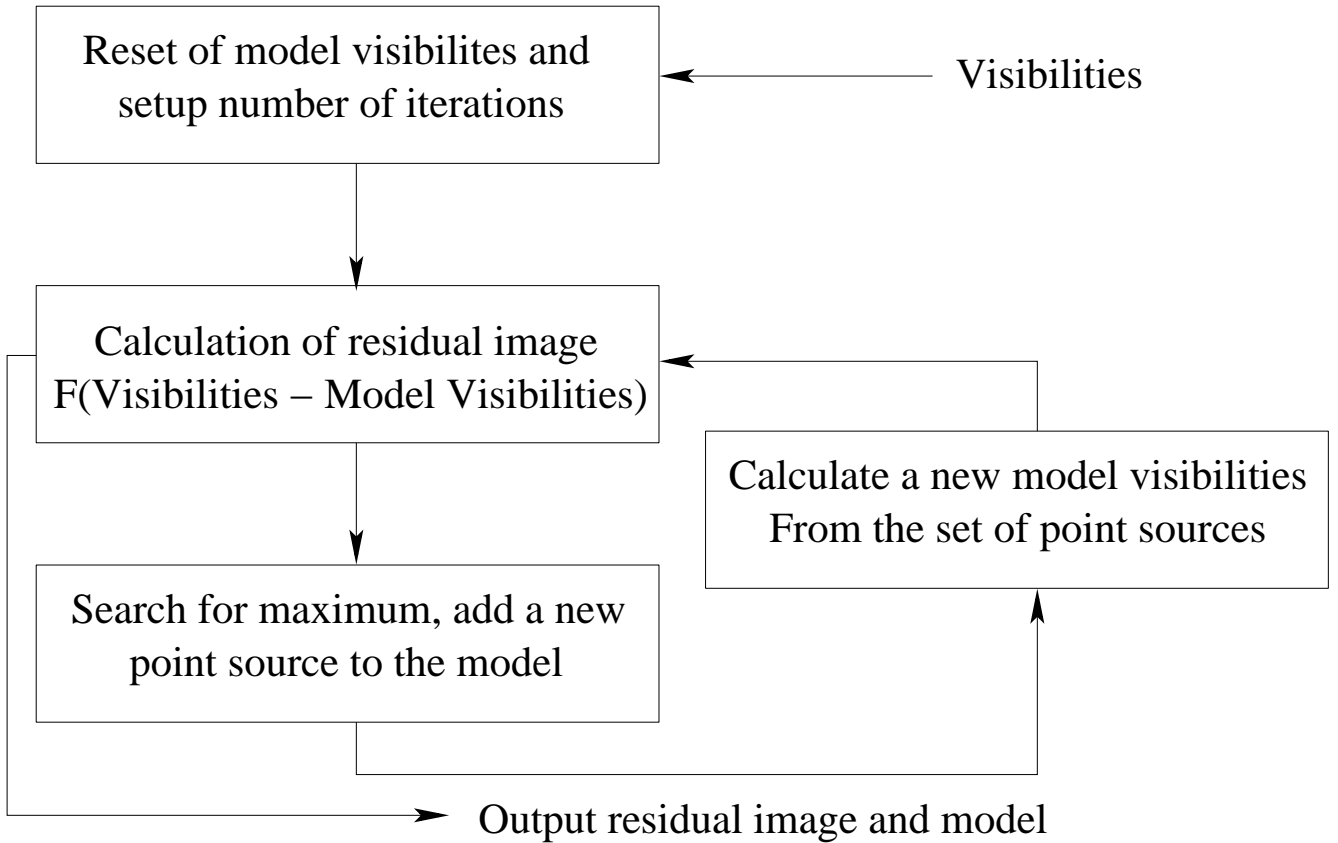


Figure 8: Flow chart explaining the Cotton-Schwab CLEAN algorithm.

sources the dynamic range will be lower because at least one of the simulated sources will be shifted from the phase-tracking centre. We assume that this decrease is due to gridding errors. The power contained in the sidelobes falling outside the field of view returns as a noise in the image. This may be notable at the extremely high dynamic ranges we are interested in. The following two facts support this idea. First, the decrease of dynamic range is less for the same shift if the image size is larger. Second, if the data were shifted to a new phase centre before the imaging stage, the dynamic range peaks at the new phase centre (Fig.7). It is possible to avoid aliasing in the subtraction of model if that subtraction is done in raw (ungridded) visibilities. This approach is called a Cotton-Schwab CLEAN algorithm (e.g. Schwab, 1984). Such an algorithm was implemented as an external program in the AIPS++/glish environment. A flow-chart explaining how it works is shown in Fig.8. At the first step model visibilities are reset to zero and the list of model components is assigned to an empty list. Further, the residual image (a dirty image from the difference of input visibilities and model visibilities) was calculated using normal FFT+gridding technique with a uniform weighting. This stage was performed using the AIPS++ imager tool. This residual image is used

to search for maximum of emission only. The value and the position of this maximum is used to update the list of model components (some fraction of the peak value called a loop gain is actually added to the model at each iteration). To complete the loop it is necessary to generate the model visibilities from the current list of model components. After a required number of iterations the current component list and the residual image form the output. The model was calculated as a sum of point source visibilities

$$V(u, v) = \sum_k A_k \exp \left( 2\pi i (ul_k + vm_k) \right). \quad (1)$$

Although dynamic range provided by Cotton-Schwab CLEAN is much higher, the dependence on the distance from the phase centre remains, however, qualitatively the same with one exception. When the data were shifted to another phase centre the CS-Clean dynamic range depends on the distance from the image center rather than on the distance from the new phase centre (see Fig.7). Presumably there are two effects degrading off-axis dynamic range, with one of them being absent for the CS-Clean (e.g. gridding errors discussed above). The equation (1) does not take into account a  $w$ -term. The relation between visibilities and a sky brightness is not actually a Fourier transform (see, e.g., Thompson, Moran and Swenson, 1986). Usually this is taken into account for wide-field imaging. However, the deviation of the true equation from the Fourier transform introduces an additional phase error which depends on the position of the source. The CS-Clean described above can be improved if the model is calculated using<sup>1</sup>

$$V(u, v, w) = \sum_k A_k \exp \left( 2\pi i \left( ul_k + vm_k + w(\sqrt{1 - l_k^2 - m_k^2} - 1) \right) \right). \quad (2)$$

In the modified CS-Clean the maximum of emission is still searched for in the residual image obtained using conventional the FFT+gridding method. However, despite these approximations, the modified CS-Clean gives an almost flat dependence of the dynamic range on the offset from the phase centre (Fig.9). Hence, it is important to take the  $w$ -term into account for ultra high dynamic range imaging even if the field of view is not large. It is not clear why the CS-Clean without  $w$ -term peaks at the centre of the image instead of the new phase centre in Fig.7. May be the implementation of AIPS++ code does not include  $w$ -term into consideration while phase-shifting the data. The dynamic range depends on the number of iterations because only a fraction (loop gain) of the peak value is subtracted at each iteration (see Fig.10). A loop gain is usually introduced in conventional CLEAN to achieve better stability of the algorithm. An additional study

---

<sup>1</sup>Amplitude reduction was not taken into consideration and may be a subject of further study.

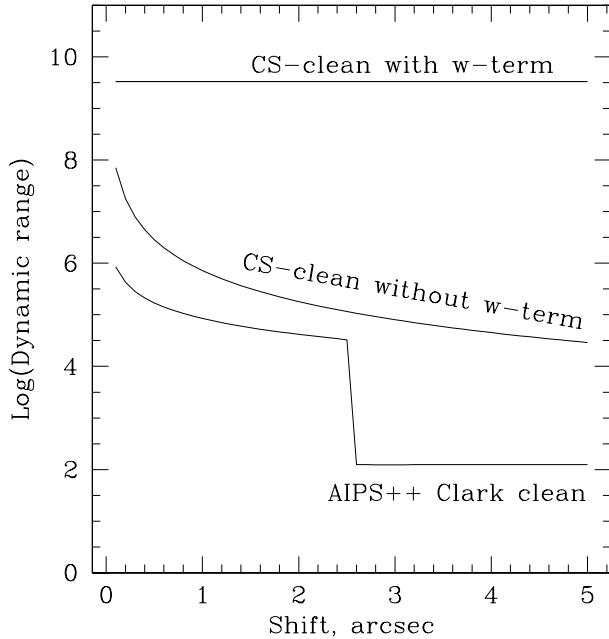


Figure 9: Dynamic range versus the offset from the phase centre for the different algorithms. Scale is logarithmic.

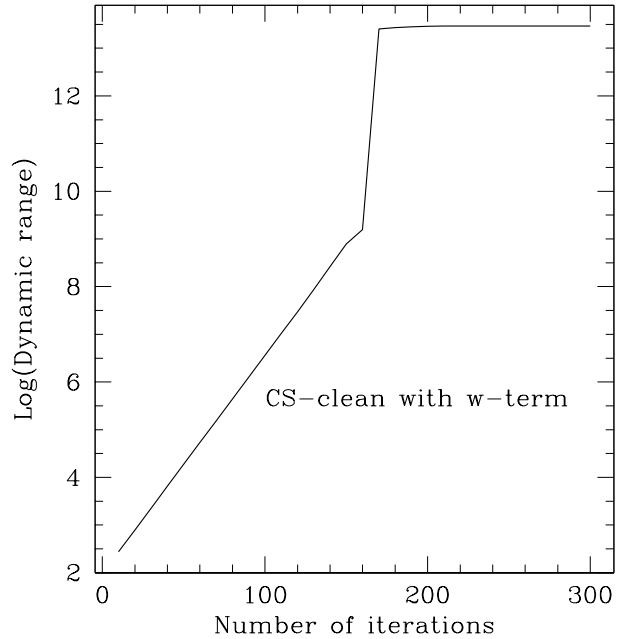


Figure 10: Dynamic range for the CS-Clean with  $w$ -term in the model of the point source at the phase centre versus the number of algorithm iterations. Loop gain is 0.1.

is required to understand the necessity or wastefulness of this approach for the raw visibility CLEAN. One can see in Fig.10 that the dynamic range depends exponentially (the scale in the figure is logarithmic) on the number of iterations when that number is relatively small. This corresponds to a geometrical progress in the cleaning of the point source

$$\text{Maximal Residual} = \text{Peak} (1 - \alpha)^{N+1}, \quad (3)$$

where  $\alpha$  is a loop gain, and  $N$  is a number of iterations. After a certain number of iterations the dynamic range increases rapidly and saturates at some level. Presumably, this level is determined by round-off errors.

### 3.3 Wide field algorithms

It is worth to say a few words about wide field deconvolution algorithms. AIPS++ provides wide field versions of different CLEAN algorithms. The general idea of such algorithms is to split the whole field of view into a number of facets each of which can be considered as a plane. For individual facets it is possible to use conventional

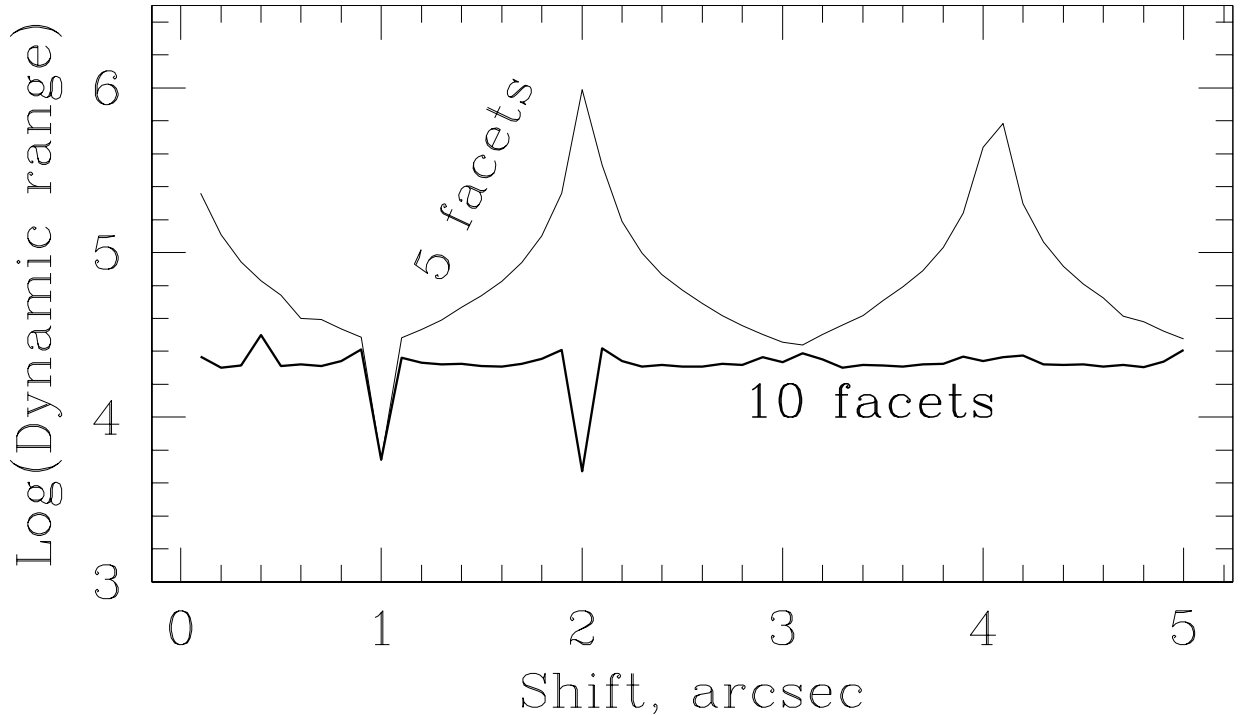


Figure 11: Dynamic range versus offset from the phase centre for the wide-field AIPS++ Clark clean for the different number of facets.

algorithms using all benefits of the Fourier transform relation. The dependence of the dynamic range on the source shift for the wide-field AIPS++ Clark clean is shown in Fig.11. One can see that the plot has a complex form presumably produced by interpolation between different facets. For the greater number of facets the curve has a more flat shape. However, the CS-Clean with  $w$ -term gives a better dynamic range. An additional study of wide-field algorithms is required because Fig.11 may simply reflect some drawbacks in the AIPS++ implementation of the algorithm instead of intrinsic limitations of the method.

## 4 Conclusions

1. For a CLEAN deconvolution to be efficient it is necessary to downweight short baselines, e.g. use the uniform weighting.
2. To achieve high dynamic ranges when the source is not in the phase centre it is necessary to take the  $w$ -term into account

3. The CS-Clean (with the  $w$ -term) gives almost equal dynamic ranges for all off-sets from the phase centre and is suitable for simulations with a complex sky brightness.
4. It is possible to reach dynamic ranges greater than  $10^8$ .

## References

Briggs D.S., High Fidelity Deconvolution of Moderately Resolved Sources, PhD thesis, The New Mexico Institute of Mining and Technology, Socorro, New Mexico, 1995

Schwab F.R., 1984, ApJ, 89, 1076

Thompson A.R., Moran J.M., Swenson G.W. Jr., Interferometry and Synthesis in Radio Astronomy, John Wiley & Sons, New York, 1986